ACS OMEGA

Open Access

This article is licensed under CC-BY-NC-ND 4.0

http://pubs.acs.org/journal/acsodf

Article

Development and Evaluation of [^{11}C]I-58: A Novel PET Radiotracer Targeting BRD4 BD2 for Advanced Epigenetic Imaging

Yanli Wang, Yongle Wang, Yulong Xu, Darcy Tocci, and Changning Wang*

Cite This: *ACS Omega* 2024, 9, 36177−36184

Read Online

ACCESS | Metrics & More | Article Recommendations | Supporting Information

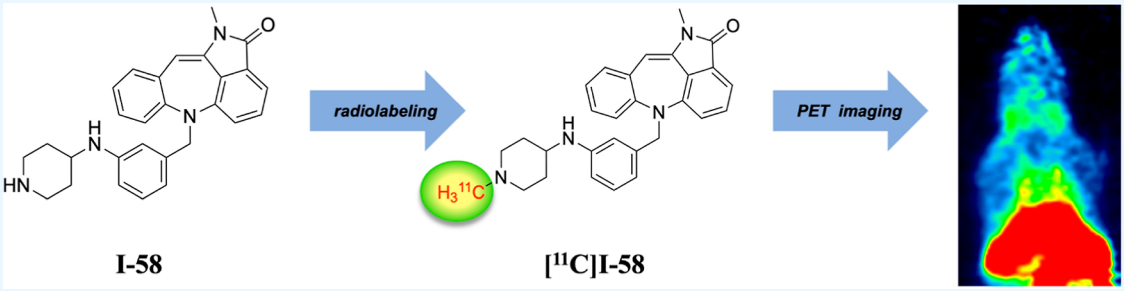

ABSTRACT: The paired bromodomains (BD1 and BD2), located in the bromodomain and extra-terminal (BET) family proteins, perform specific functions in gene transcriptional control and expression. Targeting specific bromodomains with inhibitors holds promise for achieving therapeutic benefits with reduced side effects. However, the comprehension of this target related to the disease is still restricted. Positron emission tomography (PET) imaging is a powerful tool that provides a valuable avenue for exploring the BD2 bromodomain. This investigation introduces a novel radioligand, [^{11}C]I-58, for PET targeting the BET BD2 domain. The synthesis of compound I-58, along with its radiosynthetic process for C11 labeling, is detailed, and the suitability of [^{11}C]I-58 for PET imaging of the BD2 bromodomain is evaluated. Initial PET study findings in mice indicate that [^{11}C]I-58 exhibits suitable biodistribution in peripheral organs and tissues. Additionally, in vitro autoradiography studies and blocking experiments provide compelling evidence supporting the specific binding of [^{11}C]I-58 to the BD2 bromodomain. These results establish [^{11}C]I-58 as a promising instrument for the PET imaging of the BD2 bromodomain. This research not only holds the potential to pave the path for developing PET radioligands precisely targeting the BD2 bromodomain but also adds to a more profound comprehension of the biological mechanisms linked to the BD bromodomain.

■ INTRODUCTION

The essential process of epigenetic modification, such as histone acetylation, involves the action of enzymes such as histone deacetylases (HDACs) and histone acetyltransferases. Additionally, proteins such as those in the bromodomain and extra-terminal (BET) family is related to the regulation of histone acetylation.[1,2] The BET protein family serves as a crucial epigenetic reader, significantly impacting the regulation of post translational modifications and then gene expression. This influence is exerted through their ability to recognize the acetylated lysine (KAc) residues which located on histone tails.[3,4] The BET family includes four subisoforms: BRD2, BRD3, BRD4, and BRDT, each distinguished with the presence of bromodomains BD1 and BD2, are extensively integrated into mammalian biology. BRDT is predominantly located within the testes.[5−8] Owing to their pivotal role in the modulation of epigenetic mechanisms, BET family proteins are identified as potential molecular targets for the development of therapeutic strategies. They offer potential avenues for addressing a range of conditions, including tumors, inflammation, and infectious diseases.[9,10] The BET protein family has garnered growing attention owing to its involvement in a diverse array of human diseases, with a notable focus on cancer, making it a subject of increasing interest in research and potential therapeutic development.[11] A multitude of BET inhibitors capable of inducing transcriptional changes through the disruption of interactions between bromodomains (BRDs) and acetylated lysine (KAc) have been discovered for diverse disease treatments. Since the groundbreaking identification of the initial BET inhibitor, JQ1[12,13] (Figure 1), a plethora of innovative BET inhibitors, including isoxazoles, quinoline derivatives, and tetrahydroquinolines have been developed.[14−18] Many of these BET inhibitors have been developed targeting a variety of cancer types. For instance, analogue I-BET762 demonstrates the ability to impede tumor growth

Received: February 15, 2024
Revised: April 19, 2024
Accepted: April 30, 2024
Published: August 12, 2024

ACS Publications

© 2024 The Authors. Published by American Chemical Society

https://doi.org/10.1021/acsomega.4c01495
ACS Omega 2024, 9, 36177−36184

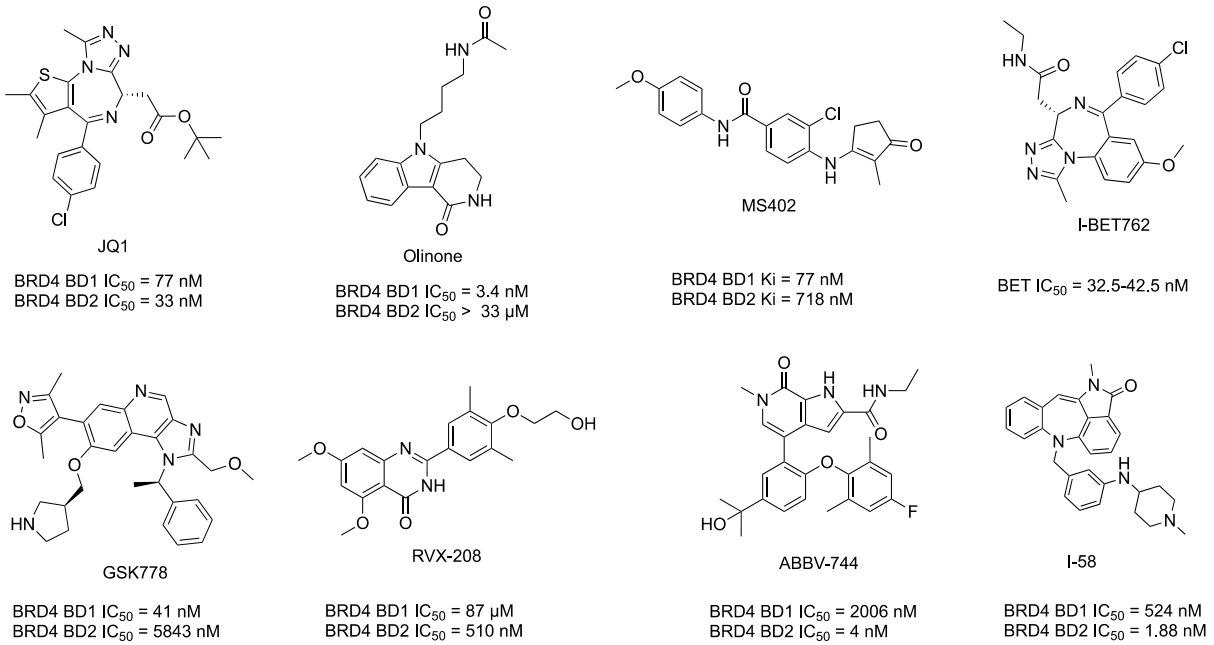

Figure 1. Molecular configurations of JQ1 and selective inhibitors targeting specific BET protein domains.

across various tumor cells by modulating the expression of the antiapoptotic gene BCL2. Currently, this entity is the subject of Phase I clinical trials aimed at evaluating its therapeutic efficacy in addressing NUT midline carcinoma and various hematological conditions.[18,19] Emerging research suggests a significant role for BET proteins in the pathology of central nervous system afflictions, encompassing neurodegenerative diseases, neural inflammation, mental health conditions, and oncological manifestations within the brain.[20] Nevertheless, the specific pathological mechanisms underlying the impact of BET proteins in neurological diseases remain unclear.[21,22]

Because of the similarity between BD1 and BD2 bromodomains, many existing BET inhibitors have been designed to probe both BD1 and BD2 simultaneously, resulting in a lack of selectivity. However, recent research has highlighted unique roles for each of BD1 and BD2 in epigenetic transcriptional regulation. Developing novel domain-selective BET inhibitors may yield an enhanced therapeutic effect and a favorable side effect profile when contrasted with simultaneous inhibition of both domains. For instance, Olinone[16] (Figure 1), a selective BET BD1 inhibitor, showed efficient myelin regeneration in neurodegenerative disorders, while RVX-208, a selective BD2 inhibitor, led to distinct gene expression alterations compared to pan-BET inhibitors.[17] Despite efforts to discover next-gen BET inhibitors, achieving high domain selectivity remains challenging, and few inhibitors show it. Additional investigation is required to comprehend the mechanisms of action associated with each bromodomain and to delve into their therapeutic potential. Within this framework, positron emission tomography (PET) serves as a prominent noninvasive modality, providing key observations pertaining to the functioning of BET BD1 and BD2 bromodomains in vivo.[23,24] Utilizing a suitable radiotracer, PET imaging has the potential to accelerate BET research, aiding researchers in disease diagnosis, treatment monitoring, and the advancement of drug development.[20] However, the design of a PET radioligand that precisely targets the BET BD1 and BD2 domains, ensuring both high affinity and specificity, remains a significant obstacle in its developmental journey.[25,26] To date, no PET radioligands have been identified that selectively target each BET subdomains for application in human subjects or for use in preclinical research. In this research, we present the conceptualization, radiolabeling process, and biological assessment of a novel BRD4 BD2-specific PET radiotracer, denoted as [^{11}C] I-58. The studies illustrate that [^{11}C] I-58 serves as a potential radioligand, exhibiting selective and specific binding to BRD4 BD2. This offers a valuable tool for quantifying, visualizing, and conducting epigenetic research on BRD4 and BD2.

Our pursuit of developing PET radiotracers with specific targeting of BET BD2 commenced with the discovery of the selective BET BD2 inhibitor Compound I-58 (1-methyl-6-(3-((1-methylpiperidin-4-yl)amino)benzyl)-1,6-dihydro-2*H*-benzo[6,7]azepino[4,3,2-*cd*]isoindol-2-one). The binding assays showed that Compound BD1−2023−01 demonstrates exceptional binding affinity and selectivity in vitro for BRD4 BD2 (IC_{50} = 1.88 nM), positioning it as a promising candidate for conversion into a PET imaging agent. This study marks the inaugural synthesis of [^{11}C] I-58, and their characterization was meticulously conducted through in vitro autoradiographic studies and in vivo dynamic PET scans in rodent models. A thorough assessment, encompassing binding specificity and brain permeability, was undertaken, providing crucial insights for the prospective development of PET radiotracers targeting BRD4 and BD2.

■ RESULTS AND DISCUSSION

Selection BRD4 BD2 Inhibitor for BET PET Imaging Probe Development. We initiated our efforts by conducting a screening of previously reported domain-selective inhibitors.[27−29] Among these candidates, we identified compounds 1−58 as robust and highly effective inhibitors of BD2. Notably, its IC_{50} value stands impressively at 1.88 nM, underscoring a remarkable selectivity factor of 279-fold when compared to BRD4 BD1.[30] Consequently, we have chosen 1−58 as a prime

https://doi.org/10.1021/acsomega.4c01495
ACS Omega 2024, 9, 36177−36184

MW	tPSA	cLog P	IC_{50} (nM)	
			BRD4 BD1	BRD4 BD2
450.59	38.82	3.933	524	1.88

Figure 2. Pharmacology and physicochemical properties of I-58.

Scheme 1. Synthetic Pathway for Reference Molecule I-58 and Precursor I-58 Pre

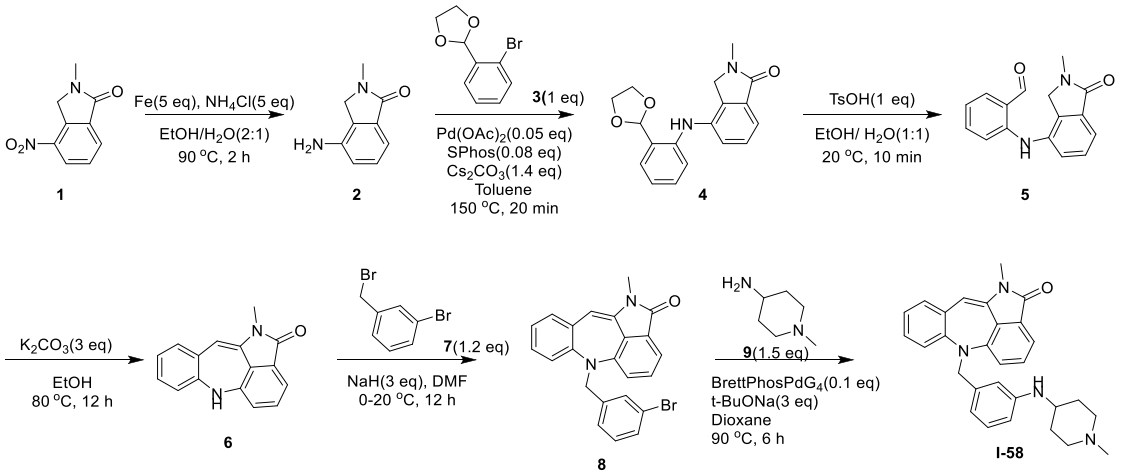

Scheme 2. Synthesis Route for the Standard Compound I-58 and I-58 Pre

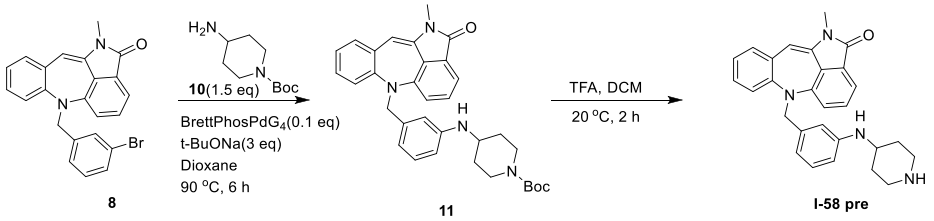

candidate for subsequent in-depth characterization and radiolabeling. Various physicochemical attributes, such as molecular weight, topological polar surface area, cLog P, and an appropriate molecular weight (typically <500) hold the potential to facilitate blood−brain barrier (BBB) penetration while minimizing nonspecific binding. These predictions collectively affirm the suitability of compounds 1−58 for radioligand development (as illustrated in Figure 2).

Chemical Synthesis for I-58, I-58 Pre, and [^{11}C]I-58. *Synthesis Summary of I-58 and I-58 Pre.* Starting from **compound 1** (2-methyl-4-nitroisoindolin-1-one) (1.8 g), a solution in EtOH and H_2O was treated with NH_4Cl and Fe at elevated temperatures (Schemes 1 and 2). The resulting mixture was filtered and extracted, yielding crude **Compound 2** (4-amino-2-methylisoindolin-1-one) (1.55 g, yellow solid, 62% yield). No purification was performed at this stage. Next, compound 2 (1.55 g) was dissolved in toluene and subjected to a Pd-catalyzed reaction with 3, s-Phos, and Cs_2CO_3 under microwave irradiation. After concentration, the residue was diluted, extracted, and purified by column chromatography, resulting in **compound 4** (4-((2-(1,3-dioxolan-2-yl)phenyl)-amino)-2-methylisoindolin-1-one) (1.4 g, yellow solid, 73%). Compound 4 (0.5 g) was then treated with TsOH·H_2O in EtOH and H_2O, giving a solution (**compound 5** (2-((2-methyl-1-oxoisoindolin-4-yl)amino)benzaldehyde)) that was directly used in the subsequent step. The mixture solution compound 5 (0.85 g) and K_2CO_3 were reacted in EtOH at elevated temperatures, followed by quenching with HCl. After extraction and purification, compound 6 (0.2 g, purple solid, 22% yield) was obtained. **Compound 6** (1-methyl-1,6-dihydro-2*H*-benzo[6,7]azepino[4,3,2-*cd*]isoindol-2-one) (0.25 g) underwent a reaction with NaH and **compound 7** (1-bromo-3-(bromomethyl)benzene) in DMF, resulting in **compound 8** (6-(3-bromobenzyl)-1-methyl-1,6-dihydro-2*H*-benzo[6,7]azepino[4,3,2-*cd*]isoindol-2-one) (180 mg, yellow solid, 36% yield) after purification by column chromatography. Finally, a mixture of compound 8 (0.12 g), **compound 9** (1-methylpiperidin-4-amine), sodium;2-methylpropan-2-olate, and Pd catalyst was subjected to a reaction in dioxane. After filtration and purification by prep-high-performance liquid chromatography (HPLC), compound I-58 (0.05 g, red solid, 32% yield, 96% purity) was obtained.

In the synthesis of I-58Pre (1-methyl-6-(3-(piperidin-4-ylamino)benzyl)-1,6-dihydro-2*H*-benzo[6,7]azepino[4,3,2-*cd*]-isoindol-2-one), a similar procedure was followed starting from **compound 8** (0.8 g), resulting in **compound 10** (*tert*-butyl 4-aminopiperidine-1-carboxylate) (0.5 g, red solid, 49% yield). **Compound 11** (*tert*-butyl 4-((3-((1-methyl-2-oxo-1,2-dihydro-6*H*-benzo[6,7]azepino[4,3,2-*cd*]isoindol-6-yl)methyl)-phenyl)amino)piperidine-1-carboxylate) was then treated with TFA and dichloromethane (DCM), and after pH adjustment and purification by prep-HPLC, compound I-58 pre (0.09 g, red solid, 99% purity) was obtained.

https://doi.org/10.1021/acsomega.4c01495
ACS Omega 2024, 9, 36177−36184

Scheme 3. Radiolabeling with I-58Pre (1 mg), [^{11}C]CH_3OTf in 0.3 mL DCM at RT for 5 min, Yielded an RCY of 11−25% (Decay-Corrected)

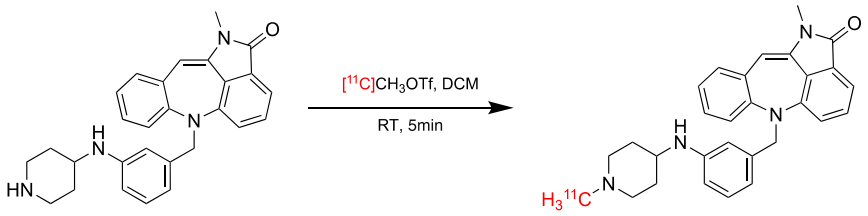

Synthesis of [^{11}C]I-58. The promising in vitro results obtained with compounds 1−58 led to the initiation of their radiolabeling studies. Illustrated in Scheme 3, we prepared [^{11}C]1−58 utilizing compound 1−58Pre as the precursor. The synthesis involved the reaction of compound 1−58Pre with [^{11}C]CH_3OTf in DCM at room temperature for 5 min. This process yielded [^{11}C]1−58 with a commendable radiochemical yield (RCY) ranging from 11 to 25% (as determined via nonspecific analysis of the trapped [^{11}C]CH_3OTf, decay corrected). Furthermore, the resultant radioligand boasted high purity and exceeded 95%.

Molecular Docking of I-58 with BRD4 BD2. The interaction mode between I-58 and BRD4 BD2 (PDB code: 6k04) was scrutinized using binding mode analysis (Figure 3).

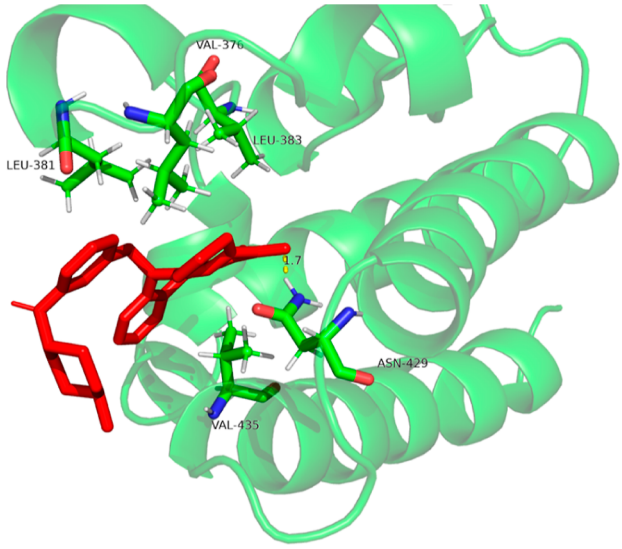

Figure 3. Molecular docking of 1−58 bound to BRD4 BD2 (PDB: 6k04), with the protein in cartoon representation and the compound and interacting residues as sticks, highlighting the hydrogen bonds in yellow.

The molecular docking results revealed significant hydrogen bonding interactions, particularly with the carbonyl group and ASN 429 residue. The binding energy of I-58 was calculated to be −7.24 kcal/mol. Additionally, I-58 exhibited hydrophobic interactions within the binding pocket, establishing bonds with VAL435, LEU381, VAL376, and LEU383. This comprehensive analysis sheds light on the specific molecular interactions that contribute to the binding affinity between I-58 and BRD4 BD2.[31,32]

In Vitro Autoradiography Study. In vitro autoradiographic investigations were performed on mouse brain sections utilizing [^{11}C]I-58 to assess its binding specificity for BRD4 BD2.[31,33] Our research, as previously detailed, involved a comprehensive in vitro autoradiographic detection process. To provide a succinct overview, mouse brain sections (sagittal plane, 20 μM thickness) underwent an initial preincubation step in a 50 mM Tris−HCl buffer solution for 20 min. Subsequently, these sections were exposed to [^{11}C]I-58 at a concentration of 1 mCi/L, also in 50 mM Tris−HCl buffer. Blocking studies involved a solution of unlabeled I-58 (10 μM) mixed with the radiotracer [^{11}C]I-58 during the incubation phase. After the incubation period, meticulous washing of the mouse brain slices with an ice-cold buffer was followed by immersion in chilled deionized water. Following this, the sections were allowed to dry naturally at ambient temperature. Autoradiographic images were captured by exposing imaging plates (BAS-MS2025, GE Healthcare, New Jersey, USA) onto desiccated cerebral slices. Autoradiographic images were produced with regions of interest (ROIs) meticulously marked out according to observed visual data. Analysis was conducted utilizing OptiQuant software from PerkinElmer, with results reported as photostimulated luminescence per square millimeter (DLU/mm^2). Figure 4 visually presents baseline and block autoradiography images of mouse sagittal brain sections with [^{11}C]I-58. Notably, the baseline signal exhibited an uneven distribution. Blocking studies of the entire brain resulted in a 40% reduction in binding. Importantly, the specific binding of [^{11}C]I-58 in key regions, including the cortex, hippocampus, thalamus, and striatum, was significantly diminished during the blockade, underscoring the tracer's specificity for these brain regions' binding sites. Encouraged by these promising ex vivo findings, we advanced to in vivo PET studies of [^{11}C]I-58.

Mouse Imaging with [^{11}C]I-58. We conducted rodent PET imaging to evaluate [^{11}C]I-58 as an in vivo imaging probe for BET BD2. The PET scans were conducted on male C57BL/6 mice, involving the intravenous administration of [^{11}C]I-58 (4.7−6.2 MBq per animal). Subsequently, a dynamic PET scan with a duration of 60 min was performed, succeeded by a computed tomography (CT) scan lasting 10 min. The dynamic PET data were compiled and subsequently reconstructed. Initially, we assessed the distribution profile of [^{11}C]I-58 across targeted organs, quantifying the radioactivity absorption rate as the percentage of injected dose per standardized uptake value (SUV). As illustrated in Figure 5, [^{11}C]I-58 predominantly accumulated in the area outside the cerebral vascular barrier. Notably, the kidneys exhibited the highest uptake of [^{11}C]I-58 among the organs of interest, with the radioactivity gradually increasing throughout the scan. Additionally, a progressive accumulation of radioactivity was observed in the liver, indicating that [^{11}C]I-58 metabolism primarily occurs in the kidney and liver. In the spleen, heart, and lung, [^{11}C]I-58 demonstrated a significant initial uptake at approximately 5 min after injection (SUV = 0.31, 0.23, and 1.05, respectively), followed by a stable uptake pattern over the 60 min scan

https://doi.org/10.1021/acsomega.4c01495
ACS Omega 2024, 9, 36177−36184

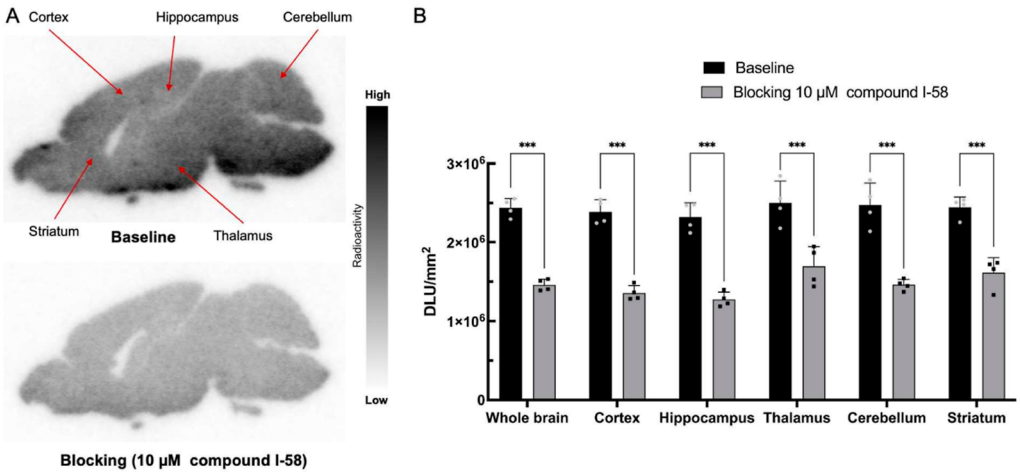

Figure 4. (A) Typical in vitro autoradiography of mouse brain slices in sagittal view; (B) comparative analysis of radiotracer uptake under baseline conditions and with blocking. Baseline sections were exposed solely to [^{11}C]I-58, whereas for blocking, sections underwent coincubation with 10 μM of compound I-58. Gray scale quantification is presented as mean ± standard deviation for four samples. Statistical significance is denoted by asterisks: ***$p \leq 0.001$.

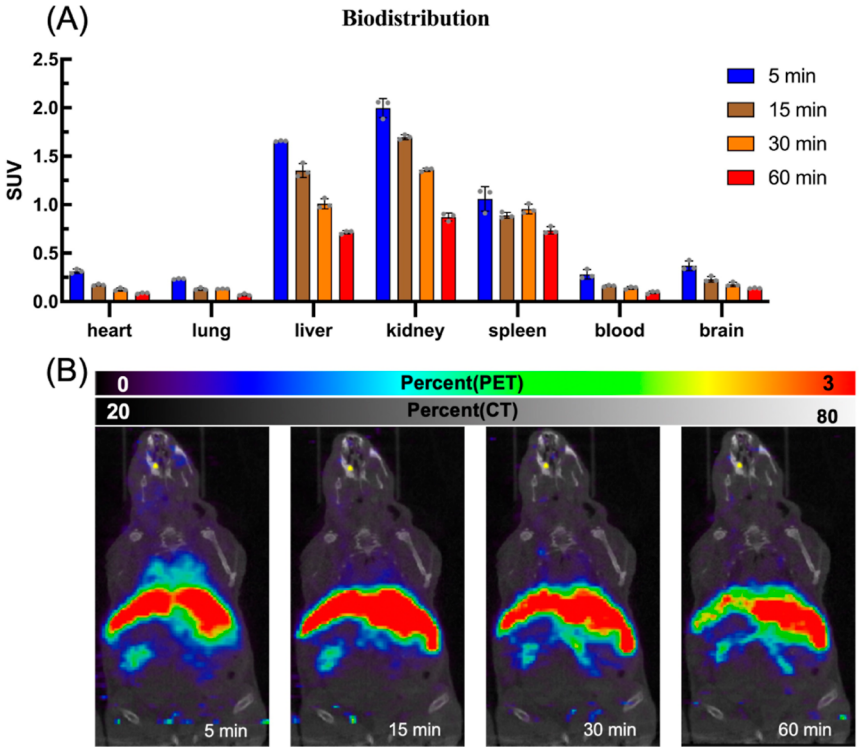

Figure 5. Biodistribution pattern of [^{11}C]I-58 in mice at different time points (5, 15, 30, and 60 min post i.v. Injection, n = 3).

duration. These observations underscore the extensive dispersion of [^{11}C]I-58 across multiple tissue types and organs. Notably, within the hepatic and renal compartments, suggesting the potential utility of [^{11}C]I-58 in PET imaging applications for disease diagnosis, including in brain diseases and tumors. The observed accumulation patterns in key organs further support the promise of [^{11}C]I-58 as a valuable tool for in vivo imaging studies related to BET BD2, contributing to an understanding of its biodistribution and metabolic pathways.

To evaluate the specific binding of [^{11}C]I-58, we conducted a comprehensive assessment of its in vivo performance within the brain, as illustrated in Figure 6. Blocking studies were done in mice, involving the administration of unlabeled I-58 (self-blocking) at concentrations of two concentrations (0.1 and 1.0 mg/kg), administered five min before the radiotracer injection. Figure 6 illustrates the outcomes of the blocking experiments alongside the time−activity curves (TACs) for the ROIs. Whole brain analysis revealed that [^{11}C]I-58 achieved peak uptake within the initial minutes postinjection, with the SUV reaching a maximum value of 0.07. Crucially, this uptake persisted throughout the entire 60 min scan period. Notably, the introduction of 0.1 mg/kg I-58 as a pretreatment substantially enhanced the uptake of [^{11}C]I-58, resulting in an average increase of 2.04 in the whole brain—effectively doubled. Similarly, the administration of 1.0 mg/kg I-58 led to an average increase of 1.72 in the whole brain. These findings

https://doi.org/10.1021/acsomega.4c01495
ACS Omega 2024, 9, 36177−36184

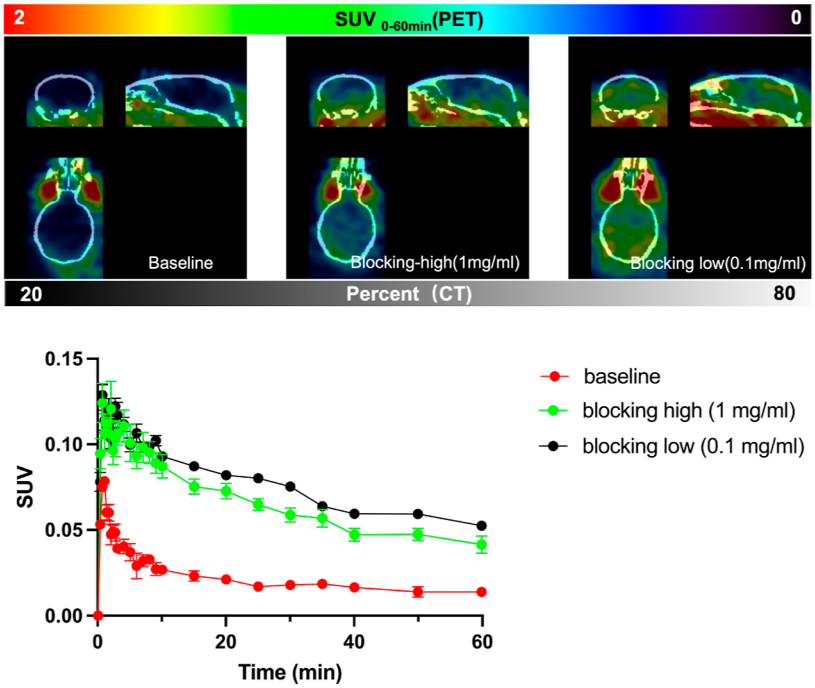

Figure 6. PET-CT imaging of mouse brain following intravenous administration of [^{11}C]I-58, focusing on the 20−60 min time frame. Additionally, it provides baseline and blocking TACs of [^{11}C]I-58, with a sample size of n = 3.

underscore the remarkable binding specificity and stability demonstrated by [^{11}C]I-58. Blocking studies played a pivotal role in elucidating the mechanism behind [^{11}C]I-58's interaction with the cerebrovascular endothelium.

The increased brain uptake in the blocking groups could be attributed to several factors. One potential explanation is that the blocking agents used in these groups may have influenced the distribution and clearance kinetics of the PET probe, suggesting that I-58 effectively binds to target proteins in the BBB, thereby facilitating greater entry of [^{11}C]I-58 into the brain. Additionally, variations in BBB permeability and regional differences in receptor expression could contribute to the observed differences. Despite this, the observed brain uptake remained relatively modest. To optimize its potential application in neuroepigenetic imaging, further refinement of the radiotracer's structure may be necessary. This could enhance its ability to penetrate the BBB, ultimately bolstering its effectiveness in neurological imaging studies.

CONCLUSIONS

In summary, we successfully designed, synthesized, and assessed the first selective BET BD2 PET radioligand, [^{11}C]I-58, through rodent PET imaging experiments. In our in vitro binding assays, our reference compound, I-58, exhibited notable affinity and specificity for BRD4 BD2. A biodistribution analysis of [^{11}C]I-58 in mice revealed significant radiotracer accumulation in peripheral tissues, notably the liver and kidneys, with detectable uptake observed in the brain. Subsequent to this, the in vitro binding specificity of [^{11}C]I-58 was assessed through blocking studies employing brain tissues from mice. In conclusion, [^{11}C]I-58 emerges as a promising lead compound for further developing the selective BET BD2 PET probe. Our ongoing efforts will be directed toward structural optimization and subsequent nonhuman primate studies to further explore its utility and translational potential.

EXPERIMENTAL SECTION

Chemistry. Compound I-58 was synthesized as below: compound 1 (1.8 g, 9.37 mmol) was dissolved in EtOH (15 mL) and H2O (7.5 mL), followed by the addition of NH4Cl (2.51 g, 46.83 mmol) and Fe (2.62 g, 46.83 mmol). The mixture was stirred at 90 °C for 2 h under N2. After filtration and extraction with H2O, the organic layers were dried and concentrated to yield compound 2. To a solution of compound 2 in Tol. (5 mL) was added compound 3, Pd(OAc)2, s-Phos, and Cs2CO3. The reaction mixture was irradiated in a microwave reactor, concentrated, and extracted with DCM. The organic layers were dried and purified to obtain compound 4. Compound 4 was then treated with TsOH to yield compound 5, which was subsequently reacted with K2CO3 in EtOH to afford compound 6. Compound 6 was reacted with NaH and compound 7 to produce compound 8, which was further reacted with compound 9 to yield compound I-58.

Compound I-58Pre was synthesized similarly, with the final step involving the reaction of compound 11 with TFA and DCM to yield compound I-58Pre. Both compounds were purified by prep-HPLC.

Radiochemistry. [^{11}C]CH_3OTf was trapped within a TRACERlab FX-M synthesizer reactor (General Electric), preloaded with 1 mg of the precursor in 1.0 mL of dry DCM. After stirring for 5 min at 25 °C, 0.5 mL of water was added. The resulting product was isolated using reverse-phase semipreparative HPLC [phenomenex Luna 5u C8(2), 250 × 10 mm, 5 μm; flow rate: 5.0 mL/min; solvent composition: 0.1% TFA in water/acetonitrile, 70/30%, v/v]. The final product was collected and loaded onto a C-18 Sep-Pak cartridge, which was then rinsed with 15 mL of water, eluted with 0.3 mL of ethanol (EtOH), and finally with 2.7 mL of saline (0.9%). The average synthesis time from the end of bombardment to the end of synthesis ranged from 30 to 35

https://doi.org/10.1021/acsomega.4c01495
ACS Omega 2024, 9, 36177−36184

min, with an average RCY ranging from 11 to 25% (activity yield corrected to trapped [^{11}C]CH_3OTf). Both chemical and radiochemical purities exceeded 95%, as determined by HPLC equipped with a UV detector and a gamma detector.

Rodent PET/CT Acquisition. The Subcommittee on Research Animal Care at Massachusetts General Hospital functions as the Institutional Animal Care and Use Committee (IACUC), overseeing and granting approval for all of the outlined procedures with thorough scrutiny. Eight male C57BL6 mice, aged 5 months, were utilized for this study. Compound I-58 1 mg was prepared for administration by dissolving it in a solution consisting of 10.0% dimethyl sulfoxide, 10.0% Tween 80, and 80.0% saline, resulting in a concentration of 1.0 mg/mL. Throughout the imaging sessions, animals were anesthetized with 1−1.5% isoflurane, maintaining anesthesia consistently during scanning. Within a single imaging session, mice were placed within a Triumph PET/CT scanner (Gamma Medica, Northridge, CA) and intravenously injected with compound [^{11}C]I-58, each receiving a dose ranging from 4700 to 6400 KBq. Prior to radiotracer administration, mice underwent a 5 min pretreatment with compound I-58 at doses of 0.5 and 2.0 mg/kg (one mouse for each dose), or vehicle alone (one mouse), via a lateral tail vein catheter. Following radiotracer injection, animals underwent a 60 min dynamic PET scan, followed by CT.

Rodent PET/CT Image Analysis. The PET data were reconstructed using a 3D-MLEM method, achieving a spatial resolution of 1 mm at full width at half-maximum. Following reconstruction, the data underwent analysis utilizing AMIDE39, an open-source medical imaging data examiner software based in Los Angeles, CA. DICOM format PET and CT images underwent additional processing in PMOD (PMOD Technologies, Ltd., Zürich, Switzerland), involving coregistration with the brain atlas.

VOIs were defined as spherical regions within the brain utilizing guidance from CT structural images and summed PET data. TACs were then exported as SUV activity for further analysis.

■ ASSOCIATED CONTENT

Supporting Information

The Supporting Information is available free of charge at https://pubs.acs.org/doi/10.1021/acsomega.4c01495.

Representative ^{1}H NMR and LC−MS data for I-58, additional representative ^{1}H NMR and LC−MS data specifically for I-58Pre, and HPLC chromatogram obtained from the coinjection of [^{11}C] I-58 and compound I-58 (PDF)

■ AUTHOR INFORMATION

Corresponding Author

Changning Wang − *Department of Radiology Massachusetts General Hospital, Harvard Medical School, Athinoula A. Martinos Center for Biomedical Imaging, Charlestown, Massachusetts 02129, United States;* orcid.org/0000-0002-2076-4193; Email: cwang15@mgh.harvard.edu

Authors

Yanli Wang − *Department of Radiology Massachusetts General Hospital, Harvard Medical School, Athinoula A. Martinos Center for Biomedical Imaging, Charlestown, Massachusetts 02129, United States*

Yongle Wang − *Department of Radiology Massachusetts General Hospital, Harvard Medical School, Athinoula A. Martinos Center for Biomedical Imaging, Charlestown, Massachusetts 02129, United States; School of Pharmacy, Minzu University of China, Beijing 100081, China*

Yulong Xu − *Department of Radiology Massachusetts General Hospital, Harvard Medical School, Athinoula A. Martinos Center for Biomedical Imaging, Charlestown, Massachusetts 02129, United States;* orcid.org/0000-0001-9024-7311

Darcy Tocci − *Department of Radiology Massachusetts General Hospital, Harvard Medical School, Athinoula A. Martinos Center for Biomedical Imaging, Charlestown, Massachusetts 02129, United States*

Complete contact information is available at: https://pubs.acs.org/10.1021/acsomega.4c01495

Author Contributions

Investigation, Y.W. and Y.W.; writing—original draft preparation, Y.W.; writing—review and editing, Y.W., Y.X., and D.T.; supervision, C.W.; project administration, C.W.; and funding acquisition, C.W. All authors have reviewed and consented to the final version of the manuscript for publication.

Notes

The authors declare no competing financial interest.

■ ACKNOWLEDGMENTS

This research was supported by the National Institute of Health grant number AG081195. The authors gratefully acknowledge the assistance of the Martinos Center radiopharmacy and imaging staff in conducting rodent experiments and radioisotope production.

■ REFERENCES

(1) Slaughter, M. J.; Shanle, E. K.; Khan, A.; Chua, K. F.; Hong, T.; Boxer, L. D.; Allis, C. D.; Josefowicz, S. Z.; Garcia, B. A.; Rothbart, S. B.; Strahl, B. D.; Davis, I. J. HDAC inhibition results in widespread alteration of the histone acetylation landscape and BRD4 targeting to gene bodies. *Cell Rep.* **2021**, *34* (3), 108638.

(2) Samanta, S.; Rajasingh, S.; Cao, T.; Dawn, B.; Rajasingh, J. Epigenetic dysfunctional diseases and therapy for infection and inflammation. *Biochim. Biophys. Acta, Mol. Basis Dis.* **2017**, *1863* (2), 518−528.

(3) Ruthenburg, A. J.; Li, H.; Patel, D. J.; Allis, C. D. Multivalent engagement of chromatin modifications by linked binding modules. *Nat. Rev. Mol. Cell Biol.* **2007**, *8* (12), 983−994.

(4) Gallenkamp, D.; Gelato, K. A.; Haendler, B.; Weinmann, H. Bromodomains and their pharmacological inhibitors. *ChemMedChem* **2014**, *9* (3), 438−464.

(5) Wang, N.; Wu, R.; Tang, D.; Kang, R. The BET family in immunity and disease. *Signal Transduction Targeted Ther.* **2021**, *6* (1), 23.

(6) Filippakopoulos, P.; Knapp, S. Targeting bromodomains: epigenetic readers of lysine acetylation. *Nat. Rev. Drug Discovery* **2014**, *13* (5), 337−356.

(7) Cheung, K. L.; Kim, C.; Zhou, M. M. The Functions of BET Proteins in Gene Transcription of Biology and Diseases. *Front Mol. Biosci.* **2021**, *8*, 728777.

(8) Cochran, A. G.; Conery, A. R.; Sims, R. J., 3rd Bromodomains: a new target class for drug development. *Nat. Rev. Drug Discovery* **2019**, *18* (8), 609.

(9) Wang, Z. Q.; Zhang, Z. C.; Wu, Y. Y.; Pi, Y. N.; Lou, S. H.; Liu, T. B.; Lou, G.; Yang, C. Bromodomain and extraterminal (BET)

proteins: biological functions, diseases, and targeted therapy. *Signal Transduction Targeted Ther.* **2023**, *8* (1), 420.

(10) Zhang, G.; Smith, S. G.; Zhou, M. M. Discovery of Chemical Inhibitors of Human Bromodomains. *Chem. Rev.* **2015**, *115* (21), 11625.

(11) Sarnik, J.; Popławski, T.; Tokarz, P. BET Proteins as Attractive Targets for Cancer Therapeutics. *Int. J. Mol. Sci.* **2021**, *22* (20), 11102.

(12) Lambert, J. P.; Picaud, S.; Fujisawa, T.; Hou, H.; Savitsky, P.; Uusküla-Reimand, L.; Gupta, G. D.; Abdouni, H.; Lin, Z. Y.; Tucholska, M.; Knight, J. D. R.; Gonzalez-Badillo, B.; St-Denis, N.; Newman, J. A.; Stucki, M.; Pelletier, L.; Bandeira, N.; Wilson, M. D.; Filippakopoulos, P.; Gingras, A. C. Interactome Rewiring Following Pharmacological Targeting of BET Bromodomains. *Mol. Cell* **2019**, *73* (3), 621−638.

(13) Filippakopoulos, P.; Qi, J.; Picaud, S.; Shen, Y.; Smith, W. B.; Fedorov, O.; Morse, E. M.; Keates, T.; Hickman, T. T.; Felletar, I.; Philpott, M.; Munro, S.; McKeown, M. R.; Wang, Y.; Christie, A. L.; West, N.; Cameron, M. J.; Schwartz, B.; Heightman, T. D.; La Thangue, N.; French, C. A.; Wiest, O.; Kung, A. L.; Knapp, S.; Bradner, J. E. Selective inhibition of BET bromodomains. *Nature* **2010**, *468* (7327), 1067−1073.

(14) Gilan, O.; Rioja, I.; Knezevic, K.; Bell, M. J.; Yeung, M. M.; Harker, N. R.; Lam, E. Y. N.; Chung, C. W.; Bamborough, P.; Petretich, M.; Urh, M.; Atkinson, S. J.; Bassil, A. K.; Roberts, E. J.; Vassiliadis, D.; Burr, M. L.; Preston, A. G. S.; Wellaway, C.; Werner, T.; Gray, J. R.; Michon, A. M.; Gobbetti, T.; Kumar, V.; Soden, P. E.; Haynes, A.; Vappiani, J.; Tough, D. F.; Taylor, S.; Dawson, S. J.; Bantscheff, M.; Lindon, M.; Drewes, G.; Demont, E. H.; Daniels, D. L.; Grandi, P.; Prinjha, R. K.; Dawson, M. A. Selective targeting of BD1 and BD2 of the BET proteins in cancer and immunoinflammation. *Science* **2020**, *368* (6489), 387−394.

(15) Cheung, K.; Lu, G.; Sharma, R.; Vincek, A.; Zhang, R.; Plotnikov, A. N.; Zhang, F.; Zhang, Q.; Ju, Y.; Hu, Y.; Zhao, L.; Han, X.; Meslamani, J.; Xu, F.; Jaganathan, A.; Shen, T.; Zhu, H.; Rusinova, E.; Zeng, L.; Zhou, J.; Yang, J.; Peng, L.; Ohlmeyer, M.; Walsh, M. J.; Zhang, D. Y.; Xiong, H.; Zhou, M. M. BET N-terminal bromodomain inhibition selectively blocks Th17 cell differentiation and ameliorates colitis in mice. *Proc. Natl. Acad. Sci. U.S.A.* **2017**, *114* (11), 2952.

(16) Gacias, M.; Gerona-Navarro, G.; Plotnikov, A. N.; Zhang, G.; Zeng, L.; Kaur, J.; Moy, G.; Rusinova, E.; Rodriguez, Y.; Matikainen, B.; Vincek, A.; Joshua, J.; Casaccia, P.; Zhou, M. M. Selective chemical modulation of gene transcription favors oligodendrocyte lineage progression. *Chem. Biol.* **2014**, *21* (7), 841.

(17) Picaud, S.; Wells, C.; Felletar, I.; Brotherton, D.; Martin, S.; Savitsky, P.; Diez-Dacal, B.; Philpott, M.; Bountra, C.; Lingard, H.; Fedorov, O.; Müller, S.; Brennan, P. E.; Knapp, S.; Filippakopoulos, P. RVX-208, an inhibitor of BET transcriptional regulators with selectivity for the second bromodomain. *Proc. Natl. Acad. Sci. U.S.A.* **2013**, *110* (49), 19754.

(18) Faivre, E. J.; McDaniel, K. F.; Albert, D. H.; Mantena, S. R.; Plotnik, J. P.; Wilcox, D.; Zhang, L.; Bui, M. H.; Sheppard, G. S.; Wang, L.; Sehgal, V.; Lin, X.; Huang, X.; Lu, X.; Uziel, T.; Hessler, P.; Lam, L. T.; Bellin, R. J.; Mehta, G.; Fidanze, S.; Pratt, J. K.; Liu, D.; Hasvold, L. A.; Sun, C.; Panchal, S. C.; Nicolette, J. J.; Fossey, S. L.; Park, C. H.; Longenecker, K.; Bigelow, L.; Torrent, M.; Rosenberg, S. H.; Kati, W. M.; Shen, Y. Selective inhibition of the BD2 bromodomain of BET proteins in prostate cancer. *Nature* **2020**, *578* (7794), 306.

(19) Shi, X.; Wang, Y.; Zhang, L.; Zhao, W.; Dai, X.; Yang, Y. G.; Zhang, X. Targeting bromodomain and extra-terminal proteins to inhibit neuroblastoma tumorigenesis through regulating MYCN. *Front. Cell Dev. Biol.* **2022**, *10*, 1021820.

(20) Zhang, J.; Wickizer, C.; Ding, W.; Van, R.; Yang, L.; Zhu, B.; Yang, J.; Zhang, C.; Shen, S.; Shao, Y.; Ran, C. In Vivo Three-dimensional Brain Imaging with Chemiluminescence Probes in Alzheimer's Disease Models. *Proc. Natl. Acad. Sci. U.S.A.* **2023**, *120*, No. e2310131120.

(21) Martella, N.; Pensabene, D.; Varone, M.; Colardo, M.; Petraroia, M.; Sergio, W.; La Rosa, P.; Moreno, S.; Segatto, M. Bromodomain and Extra-Terminal Proteins in Brain Physiology and Pathology: BET-ing on Epigenetic Regulation. *Biomedicines* **2023**, *11* (3), 750.

(22) Singh, M. B.; Sartor, G. C. BET bromodomains as novel epigenetic targets for brain health and disease. *Neuropharmacology* **2020**, *181*, 108306.

(23) Bai, P.; Lan, Y.; Wang, H.; Chen, Z.; Fiedler, S.; Striar, R.; Lu, X.; Wang, C. Development of a Novel Positron Emission Tomography (PET) Radiotracer Targeting Bromodomain and Extra-Terminal Domain (BET) Family Proteins. *Front Mol. Biosci.* **2020**, *7*, 198.

(24) Xu, Y.; Wang, Y.; Wang, H.; Wang, C. Synthesis and Characterization of Carbon-11 Labeled Iloperidone for Imaging of α(1)-Adrenoceptor in Brain. *Front Mol. Biosci.* **2020**, *7*, 586327.

(25) Yang, J.; Zhu, B.; Ran, C. The Application of Bio-orthogonality for In Vivo Animal Imaging. *Chem. Biomed Imaging.* **2023**, *1* (5), 434−447.

(26) Wang, Y.; Wang, Y.; Liu, Y.; Cheng, H.; Dagnew, T. M.; Xu, Y.; Wang, C. Synthesis and Characterization of a New Carbon-11 Labeled Positron Emission Tomography Radiotracer for Orexin 2 Receptors Neuroimaging. *Drug Des., Dev. Ther.* **2024**, *18*, 215−222.

(27) Bradley, E.; Fusani, L.; Chung, C. W.; Craggs, P. D.; Demont, E. H.; Humphreys, P. G.; Mitchell, D. J.; Phillipou, A.; Rioja, I.; Shah, R. R.; Wellaway, C. R.; Prinjha, R. K.; Palmer, D. S.; Kerr, W. J.; Reid, M.; Wall, I. D.; Cookson, R. Structure-Guided Design of a Domain-Selective Bromodomain and Extra Terminal N-Terminal Bromodomain Chemical Probe. *J. Med. Chem.* **2023**, *66*, 15728−15749.

(28) Divakaran, A.; Harki, D. A.; Pomerantz, W. C. K. Recent progress and structural analyses of domain-selective BET inhibitors. *Med. Res. Rev.* **2023**, *43* (4), 972−1018.

(29) Fu, Y.; Zhang, Y.; Sun, H. Progress in the development of domain selective inhibitors of the bromo and extra terminal domain family (BET) proteins. *Eur. J. Med. Chem.* **2021**, *226*, 113853.

(30) Yadong, L. T. C.; Li, H.; Jiang, F.; Ren, J.; Wang, Z.; Cui, Y. InventorAzepane[4,3,2-cd]isoindol-2-one derivatives Objects and their applications, CN113135922A.

(31) Koepp, M. J.; Hand, K. S.; Labbé, C.; Richardson, M. P.; Van Paesschen, W.; Baird, V. H.; Cunningham, V. J.; Bowery, N. G.; Brooks, D. J.; Duncan, J. S. In vivo [11C]flumazenil-PET correlates with ex vivo [3H]flumazenil autoradiography in hippocampal sclerosis. *Ann. Neurol.* **1998**, *43* (5), 618.

(32) Wang, Y.; Yao, Y.; Liu, J.; Wu, L.; Liu, T.; Cui, J.; Lee, D. Y. Synthesis and Biological Activity of Piperine Derivatives as Potential PPARγ Agonists . *Drug Des., Dev. Ther.* **2020**, *14*, 2069.

(33) Duncan, J. S. Positron emission tomography receptor studies. *Adv. Neurol.* **1999**, *79*, 893.

https://doi.org/10.1021/acsomega.4c01495
ACS Omega 2024, 9, 36177−36184